Energy Conversion and Management 210 (2020) 112698

Contents lists available at ScienceDirect

Energy Conversion and Management

journal homepage: www.elsevier.com/locate/enconman

Sulfonated functionalization of carbon derived corncob residue via hydrothermal synthesis route for esterification of palm fatty acid distillate

S. Fadhilah Ibrahim[a,b], N. Asikin-Mijan[c,*], M. Lokman Ibrahim[d,e], G. Abdulkareem-Alsultan[f], Saiman Mohd Izham[a,b], Y.H. Taufiq-Yap[a,g,*]

[a] Catalysis Science and Technology Research Centre (PutraCAT), Faculty of Science, Universiti Putra Malaysia, 43400 UPM Serdang, Selangor, Malaysia
[b] Department of Chemistry, Faculty of Science, Universiti Putra Malaysia, 43400 UPM Serdang, Selangor, Malaysia
[c] Department of Chemical Sciences, Faculty of Science and Technology, Universiti Kebangsaan Malaysia, 43600 UKM Bangi, Selangor Darul Ehsan, Malaysia
[d] Centre for Nanomaterials Research, Institute of Science, Universiti Teknologi MARA, 40450 Shah Alam, Selangor, Malaysia
[e] School of Chemistry and Environment, Faculty of Applied Sciences, University Teknologi MARA, 40450 Shah Alam, Selangor, Malaysia
[f] Chemical and Environmental Engineering Department, Faculty of Engineering, Universiti Putra Malaysia, 43400 UPM Serdang, Selangor, Malaysia
[g] Chancellery Office, Universiti Malaysia Sabah, 88400 Kota Kinabalu, Sabah, Malaysia

ARTICLE INFO

Keywords:
Biodiesel
Corncorb
Esterification
Hydrothermal
PFAD

ABSTRACT

Low-cost biodiesel was successfully produced through esterification of palm fatty acid distillate over corncob residue-derived heterogeneous solid acid catalyst. The sulfonated functionalized carbon derived from corncob was synthesized via hydrothermal carbonization followed by chemical activation using concentrated sulfuric acid. This technique allows efficient carbonization process and able to maintain active polar species of the catalyst hence effectively improves the acid strength of prepared catalyst. The esterification of palm fatty acid distillate over HTC-S catalyst was optimized via the one-variable-at-a-time technique, and 92% free fatty acid conversion with a biodiesel yield of 85% was achieved at optimum conditions of 2 h reaction time, 70 °C reaction temperature, 3 wt% catalyst loading, and 15:1 methanol-to-oil molar ratio. Various of catalyst regeneration techniques have been studied and sulfuric acid treatment is found to be the most effective approach for restoring the active sites for spent HTC-S catalyst in comparison to washing solvent and thermal treatment. The HTC-S catalyst regenerated via sulfuric acid treatment is capable to convert PFAD to biodiesel with free fatty acid conversion > 90% for two consecutive cycles. The synthesized PFAD-derived biodiesel has complied with the international biodiesel standard ASTM D6751.

1. Introduction

Biodiesel is a mono alkyl ester of long chain fatty acids, also known as fatty acid methyl ester (FAME), produced via esterification and transesterification of edible and non-edible vegetable oils in the presence of an acidic or basic catalyst with short chain alcohols [1–3]. Due to its non-toxicity, biodegradability, and clean emissions (including low HCs, CO, and particulates), biodiesel is an ideal alternative renewable energy resource to replace petroleum-derived diesel fuel [4]. Homogeneous catalysts, such as NaOH, KOH, H_2SO_4, and H_3PO_4, are often used in biodiesel production. However, homogeneous catalysts present a number of disadvantages, such as non-reusability and generation of large amounts of waste and effluents [5,6]. Furthermore, homogeneous catalysts can cause engine corrosion [7]. As such, the use of heterogeneous catalysts for biodiesel production has gained increased attention for its ability to cope with most of the economic and environmental drawbacks of a homogeneous process [8].

Utilization of an inexpensive and low-quality feedstock, particularly palm fatty acid distillate (PFAD) for biodiesel production has been studied by a number of researchers [9]. PFAD appears as yellow solid at room temperature and turns light brown upon melting; it is directly produced during the refining of crude palm oil after fatty acid stripping and deodorization. PFAD is composed of approximately 98% free fatty acids (FFAs); the majority of its components consist of palmitic acid (C16:0) and oleic acid (C18:1), and its remaining components are triglycerides and partial glycerides [10]. In 2019, Malaysia, as the second largest crude palm oil producer in the world, produced approximately 776,500 metric tons of PFAD (MPOB, 2014). Due to large availability

* Corresponding authors at: Department of Chemical Sciences, Faculty of Science and Technology, Universiti Kebangsaan Malaysia, 43600 UKM Bangi, Selangor Darul Ehsan, Malaysia (N. Asikin-Mijan). Catalysis Science and Technology Research Centre (PutraCAT), Faculty of Science, Universiti Putra Malaysia, 43400 UPM Serdang, Selangor, Malaysia, and Chancellery Office, Universiti Malaysia Sabah, 88400, Kota Kinabalu, Sabah, Malaysia (Y.H. Taufiq-Yap).
E-mail addresses: nurul.asikin@ukm.edu.my (N. Asikin-Mijan), ncums@ums.edu.my, taufiq@upm.edu.my (Y.H. Taufiq-Yap).

https://doi.org/10.1016/j.enconman.2020.112698
Received 30 December 2019; Received in revised form 4 March 2020; Accepted 5 March 2020

and economically competitive of PFAD hence it may provide a promising feedstock option for the production of biodiesel. Due to high FFA content of PFAD, thus PFAD-derived biodiesel is predominantly produced via catalyzed esterification reaction over a heterogeneous solid acid catalyst.

A number of scholars have assessed the use of biomass-derived carbon-catalysts in the esterification reaction; here, the carbon is initially synthesized via carbonization of biomass at temperature exceeding 700 °C [11]. However, this method is unable to produce high-quality carbon, requires high energy consumption, and entails high costs; as such, its large-scale productions are limited. The hydrothermal carbonization technique may offer an efficient solution to these issues. In this process, carbon is formed at low temperature (< 200 °C) under closed high-pressure conditions. This step is important as it could maintains the active polar oxygenated functionalities in the biomass [12]. The key step to improve the acidic sites on carbon is chemical activation, where carbon is treated with a chemical agent, such as H_3PO_4, H_2SO_4, HCl, or $HClSO_3$ [13,14]. Chen and Fang demonstrated that sulfonated amorphous carbon with $^{-}SO_3H$ groups in its structure presents much higher catalytic esterification activity than other solid acid catalysts [15]. Moreover, Santos et al. also revealed that sulfonation activation results in carbon with high adsorption capacity, which favors esterification reactivity [16].

Corn (*Zea mays* L.) is the third largest agricultural crop in the world after wheat and rice. Corn is grown around the world, including Northern America, Asian, Europe, and Latin America, and largely consumed by humans and animals [17]. The massive production of corn translates to the excessive production of corncob residue, which is generally dumped and burned off, thus causing gross air pollution. Corncob is rich in hemicellulose polysaccharides (30%–40%), which have very important applications in the food industry and biofuels [18]. Hemicellulosic polysaccharides can be thermally treated and chemically functionalized into acidic carbon-based catalysts. Production of functionalized carbon-based corncob-derived catalysts via thermal activation (> 700 °C) followed by chemical activation for biodiesel production has been widely reported [1]. However, no study describing functionalized carbon-based catalysts derived from corncob residue and produced via hydrothermal carbonization technique for biodiesel production has yet been published. In view of this knowledge gap, this is the first report discussed on the development of the functionalized carbon catalyst derived from corncob residue by hydrothermal technique for the esterification of PFAD. Detailed characterization of the synthesized catalysts was conducted, and the effects of catalyst concentration, oil-to-methanol molar ratio, reaction temperature, and reaction time on the rate of the esterification of PFAD were evaluated via one-variable-at-a-time (OVAT) techniques. The properties of the PFAD-derived biodiesel analyzed by a gas chromatography–flame ionization detector (GC-FID), and the reusability profile of sulfonated carbon derived from corncob residue was assessed.

2. Experimental

2.1. Materials and chemicals

Corncob residue was collected form night market at Serdang, Malaysia. The concentrated Sulfuric acid H_2SO_4 with purity 98%, was purchased from Sigma-Aldrich (USA). The solvent methanol (MeOH) 99.8% of analytical grades was purchased from J.T. Baker. The solvent such as ethanol, hexane and acetone were supplied by Merck & Co., USA. The PFAD was obtained from Jomalina R&D, SIME DARBY Co., Malaysia. The reference standard of FAMEs (methyl oleate, methyl linoleate, methyl palmitate, methyl myristate and methyl stearate) and internal standard (methyl heptadecanoate) with purity ≥99% was obtained from Fluka Analytical. The *n*-hexane (GC grade) was purchased from Supra Solv Merck. Palm fatty acid distillate (PFAD) were obtained from Jomalina R&D, Sime Darby Co., Klang, Malaysia and the properties of PFAD feedstock were analyzed according to American Oil Chemist's Society (AOCS) and British Standard methods. The properties of PFAD were tabulated in Table 1.

Table 1
The properties of PFAD, data are presented as mean ± standard deviation.

Properties	Method	Result
FFA content (Palmitic %)	AOCS Cd 3d-63	98.9 ± 0.71
Saponification value (mg KOH/g)	AOCS Tr 1a-64	197 ± 3.32
Molecular weight (g mol^{-1})[a]		193.2
Fatty acid composition (wt%)		
Myristic (C14:0)		1.08 ± 0.05
Palmitic (C16:0)		58.92 ± 0.32
Stearic (C18:0)		3.24 ± 1.01
Oleic (C18:1)		30.34 ± 1.32
Linoleic (C18:2)		6.42 ± 0.71
Σ Unsaturated		63.24
Σ Saturated		36.76

[a] Obtained from the fatty acid composition.

2.2. Catalyst preparation

The sulfonated functionalized carbon derived from corncob was synthesized using a three-step process: mechanical grinding followed by hydrothermal carbonization and chemical activation. Briefly, corncob were grind into a small-sized aggregates shaped with a diameter (1–2 cm) by a mini milling machine 1250 g Multi-function disintegrator (220–240 V~, 3500 W, 50–60 Hz, n_o25,000 r/min) for 2 min (Fig. 1a). The aggregates-shaped corncob directly undergoes hydrothermal carbonization by mixing 5 g of aggregates-shaped corncob with 100 mL distillate water and loaded into the autoclave followed by gently heated to 200 °C for 10 h. The treated aggregates-shaped corncob was filtered, washed with distilled water till pH = 7 at room temperature prior to drying at 100 °C for 12 h. The dried sample were later crushed to obtain fine powder and denoted as HTC. The HTC powder was later further treated with 100 mL of sulfuric acid under reflux system at 150 °C for 8 h. The slurry is filtered and washed with hot distillate water (80 °C) till pH = 7 in order to remove unreacted sulfuric acid and dried for 1 h at 100 °C. The obtained powder was denoted as HTC-S.

2.3. Catalyst characterization

An X-ray diffractometer (XRD; Model XRD 6000, Shimadzu) was used to study the structures of the synthesized samples. The instrument employed Cu-Kα radiation (λ = 0.15406 nm) at 30 kV and 15 mA, and scans were conducted over the 2θ range of 20°–80° with a scanning rate of 2° min^{-1}. The Brunauer–Emmet–Teller (BET) model was used to determine the surface area and pore distribution of the catalysts with a Sorptomatic 1990 series instrument (Thermo Finnigan). Pore diameter distributions were determined by the Barrett–Joyner–Halenda technique from the desorption loop. The functional groups of the catalyst were studied by using Fourier transform infrared (FTIR) spectroscopy with a Perkin Elmer 1650 spectrometer; peaks were recorded in the range of 400–4000 cm^{-1}. Temperature-programmed desorption of ammonia (TPD-NH_3) was used to identify the total acidity of catalysts that had been pre-treated under a N_2 environment to remove moisture and impurities. The pre-treated catalysts were saturated with NH_3 for 1 h and then flushed with N_2 at a rate of 30 $mLmin^{-1}$ The N_2-absorbing catalysts were heated from 50 °C to 900 °C, and the desorbed gas was interpreted by using a TPD/R/O 1100 instrument (Thermo Finnigan). Field-emission scanning electron microscopy (FESEM; JEOL JSM-7600F) was used to examine the morphology of the catalysts. The elemental composition of fresh and spent HTC-S catalysts were also further determined by field emission scanning electron microscopy (FESEM) fitted with EDX analysis using Rayny EDX-720 spectrometer and Jeol JSM-7600F. A CHNS/O analyzer (TruSpec, LECO) was used to

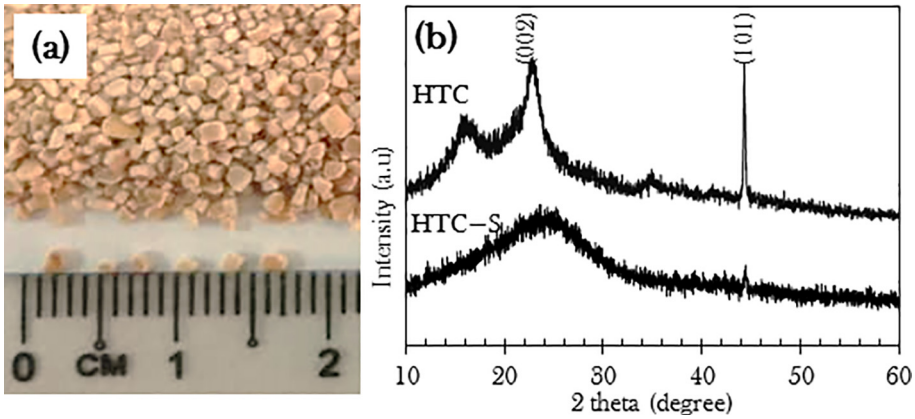

Fig. 1. (a) Corncob image after milling process (b) XRD patterns of the HTC and HTC–S catalysts.

determine total amount of carbon, hydrogen, nitrogen, sulfur, and oxygen in the biodiesel.

2.4. Esterification of PFAD

The esterification reaction was carried out in a 150 mL two-necked round-bottom flask equipped with a reflux condenser and a magnetic stirrer. Approximately 10 g of PFAD, the required amount of synthesized catalyst, and methanol were mixed and then refluxed at 70 °C in an oil bath for a certain time under vigorous stirring. The solution was then centrifuged to separate the solid catalyst and the mixture of methanol and biodiesel. The acid values of PFAD and biodiesel were determined according to AOAS Cd 3d-63 standard (Eq. (1)). The FFA conversion of the collected product was determined by using European standard method EN 14,103 method; Eq. (2). The composition of PFAD and biodiesel were determined by using a GC–MS QP2010 Plus instrument (Shimadzu). The biodiesel also was analyzed by using a gas chromatograph (GC-7890A, Agilent, Japan) equipped with a flame ionization detector (GC-FID; GC-14C). FAMEs were separated by using a highly polar HP-Innowax column (Agilent; length 30 m, i.d. 0.32 mm, diameter 0.25 μm). The liquid product was diluted to 500 ppm with GC-grade *n*-hexane (purity > 98.0%). Methyl heptadecanoate was used as the internal standard. Methyl oleate, methyl palmitate, methyl linoleate, methyl myristate, and methyl stearate were used as reference standards. Hexane was used as the solvent, and helium was used as the carrier gas. Approximately 1 μL of mixtures was injected into the chromatograph at a split ratio of 1:50 and injector temperatures ranging from 60 °C to 250 °C with a heating rate of 10 °C min^{-1}. The temperature at the injector port was set to 250 °C, and the detector temperature was programmed to 270 °C. Biodiesel or FAME yields were calculated according to the European standard method EN14103 using Eqs. (3)–(5). The example GCFID calculations were displayed in Fig. S1. The response factor (RF) was calculated for each compound by using a standard compound (methyl heptadecanoate) according to Eq. (3). Then, FAMEs were calculated by using Eq. (4) and FAME yield (%) using Eq. (5).

$$Acid\ \ value\ \ (AV) = \frac{A \times N \times 56.11 g/mol}{w} \tag{1}$$

A represents the volume (mL) of KOH used, N refers to the normality of KOH, 56.11 g/mol is the molar mass of KOH, and w is the mass of the sample (g).

$$FFA\ \ conversion, \% = \left(\frac{AV_f - AV_p)}{AV_f}\right) \times 100\% \tag{2}$$

AV_f and AV_p represent for the acid values of the feedstock and product, respectively.

$$Rf, \% = \frac{A_{IS} C_{rs}}{A_{rs} C_{IS}} \tag{3}$$

where A_{IS} = area of the internal standard, C_{IS} = concentration of the internal standard, A_{rs} = area of the standard reference, and C_{rs} = concentration of the standard reference. The RF value of the reference standard was used for all the samples to calculate the FAME yield (%)

$$FAME = \frac{C_{iss} A_{if} R_f}{A_{ISS}} \tag{4}$$

where C_{iss} = concentration of the internal standard in the sample, A_{iss} = area of the internal standard in the sample, and A_{if} = area of the individual FAME compound in the sample. The biodiesel yield (%) was calculated according to Eq. (5):

$$FAME\ \ yield\ \ (\%) = \frac{mass\ \ of\ \ FAME\ \ in\ \ the\ \ product\ \ calculated\ \ by\ \ GC\ \ (g)}{mass\ \ of\ \ FAME\ \ collected\ \ (g)} \times 100 \tag{5}$$

The esterification experiments were carried out thrice to confirm the reproducibility of the reaction.

2.5. Catalyst reusability

The catalyst reusability test was carried out to study the deactivation and recyclability of the catalyst. Catalysts from each cycle were recovered by simple washing with methanol or hexane and dried at 80 °C for the next reaction cycle. Washing is required to remove polar and non-polar compounds on the surface of the spent catalyst. The spent catalyst was also regenerated by hexane washing followed by regeneration with 5% or 98% H_2SO_4 and then drying in oven at 80 °C. The catalyst was treated with acid for 3 h at 150 °C and then washed once more with distilled water (> 80 °C) until pH = 7. Thereafter, the catalyst was dried in the oven and used for the next esterification reaction. Changes in the mass of the regenerated H_2SO_4-treated catalyst also were investigated. The stability of catalyst also further studied via thermal treatment, whereby the catalyst further calcined at temperature 100–300 °C for 2 h and further tested in the reusability test. Similarly, the catalysts from each cycle were recovered by hexane washing and dried at 80 °C for the next reaction cycle. Sulfur leaching species in the biodiesel were determined by using a CHNOS elemental analyzer.

3. Result and discussion

3.1. Catalyst characterizations

Fig. 1b illustrates the XRD patterns of the HTC and HTC-S catalysts.

Table 2
Textural properties and total acidity for HTC and HTC-S catalysts.

Catalyst	Surface area (m^2/g)[a]	Total pore volume (cm/g)[b]	Mean pore diameter (nm)[c]	Crystallite size (nm)[d]	Temperature desorption (°C)[e]	Total amount of acidity (mmol/g)[e]
HTC	8.76	0.065	29.50	83.12	361	12.59
HTC-S	8.40	0.055	26.32	62.36	120	2.63
					550	13.00

[a] BET surface areas were determined from Brunauer, Emmet and Teller method.
[b] Total pore volumes were determined at P/Po = 0.99 on the nitrogen adsorption isotherms.
[c] Mean pores diameter were calculated from the nitrogen desorption branch, using the BJH technique.
[d] Average crystallite size were calculated from the values of the FWHM of the (3 1 1) direction, using the Scherrer equation.
[e] Determined based on NH_3-TPD measurements.

The XRD pattern of HTC showed graphitic structures at 2θ=23° and 45°, which are assigned to the carbon planes of (0 0 2) and (1 0 1), respectively [19]. The peak of HTC impurities (2θ = 16°) disappeared in the HTC-S spectrum. After sulfonation, the HTC-S catalyst showed a typical amorphous structure with a broad peak at 2θ = 25°. This result reveals the HTC-S consists of polycyclic aromatic carbon rings oriented in a random fashion. According to Farabi et al., finding [20], it can be suggested that carbonization of HTC followed by acid treatment with a strong acid could cleave C−O−C bonds in the carbon precursor and renders HTC-S to be more rigid and amorphous than HTC due to the increased disorder of carbon sheets. Overall, broader and less intense graphite peaks were observed in the spectrum of HTC-S, which suggests that sulfonation disperses the graphitic carbon structure of the catalyst [21]. Moreover, reductions in peak intensity could be attributed to the attachment of $-SO_3H$ groups to the sp^2 carbon network, which leads to increased disorder among graphitic carbon sheets [22]. This finding in agreement with the average crystallite size calculated by the Debye–Scherrer equation at the most intense peak 2θ = 45° (Table 2). The crystallite size of HTC-S is smaller than that of HTC. Compared with that of HTC, the spectrum of HTC-S showed no other characteristic peaks besides that of the carbon (1 0 1) plane, which suggests that the latter has a higher degree of carbonization and larger carbon sheets than the former.

The BET surface area and pore properties of HTC and HTC-S are summarized in Table 2. The surface area of HTC-S was found almost identical with HTC, which indicated that insertion of $^{-}SO_3H$ groups into the surface of the carbon precursor did not give significant impact on the BET surface area of the catalyst. This finding contradicts Lokman et al. (2015), who revealed that carbon activation via thermal treatment with concentrated H_2SO_4 caused significant change on the surface area of the catalyst [19]. In the case of pore volume and pore diameter, the pore properties of HTC-S deteriorated slightly after the treatment of H_2SO_4. Here, it was speculated that H_2SO_4 treatment results in greater dispersion of $-SO_3H$ groups, which are incorporated within the pores of the HTC-S surface and cause pore blockage [23].

Fig. 2a depicts the IR spectra of all catalysts. HTC and HTC-S showed absorption bands at 1588 and 1602 cm^{-1} which were attributed to aromatic ring C=C stretching variations of polyaromatic carbon. Absorption bands at 1693 and 1695 cm^{-1} could be assigned to the C=O stretching mode of −COOH groups, which indicate the presence of acidic groups [23]. HTC showed an intense C−O peak at 1038 cm^{-1} associated by the carbonization of hemicellulosic polysaccharides in corncob [24]. The presence of $-SO_3H$ groups covalently bonded to the polyaromatic carbon structure of HTC-S was confirmed by strong vibration bands at 1028 and 1149 cm^{-1}, which are respectively associated with asymmetric and symmetric stretching modes of C−O−SO_3H [25]. The broad intense peak at 3400 cm^{-1} reflects a reduction in the stretching vibrations of hydroxyl groups (−OH) from the phenol moiety of the HTC catalyst after sulfonation treatment. Reduction of the −OH peak intensity indicates that H_2SO_4 acts as a dehydrating agent [26]. Similarly, the broad intense band at approximately 2920 cm^{-1} in the HTC-S spectrum is due to reductions in asymmetric C−H stretching after sulfonation. The presence of this peak indicates that chemical activation removes a significant amount of hydrogen from the catalyst.

The distribution of acid sites and acidic strength of HTC and HTC-S were confirmed by the TPD-NH_3 in Fig. 2b and Table 2. The NH_3 desorption profile of HTC showed peak T_{max} = 361 °C, which corresponds to a moderate number of acid sites with total acid density ~12.59 mmol/g. By comparison, HTC-S showed both weak desorption and strong acidic sites (Bronsted acid sites) at T_{min} = 120 °C and T_{max} = 550 °C with total acid density were 2.64 mmol/g and 13.00 mmol/g respectively. Zhang and co-workers reported that sulfonation treatment results in an increase in $-SO_3H$ species, which, in turn, increase the strength of acidic sites [27]. This finding is in good agreement with the results of Dawodu, who demonstrated that the acidic strength of a catalyst is enhanced by strong interactions between the $-SO_3H$ group and the graphite layer [28]. The presence of weak acid sites on HTC-S is accordance with the weak absorption peak of −OH functional group in the FTIR study (Fig. 2a) [29]. Overall, the

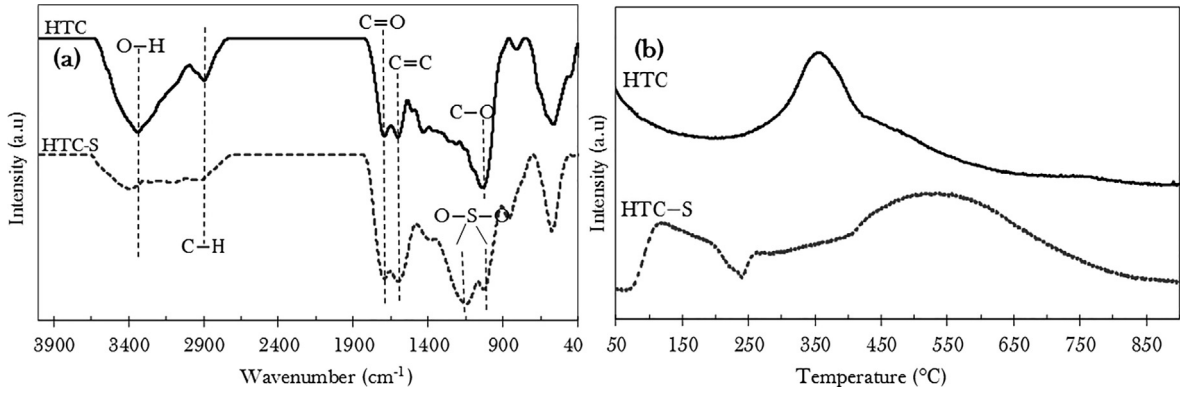

Fig. 2. The (a) FTIR spectra and (b) TPD-NH_3 profiles for the HTC and HTC–S catalysts.

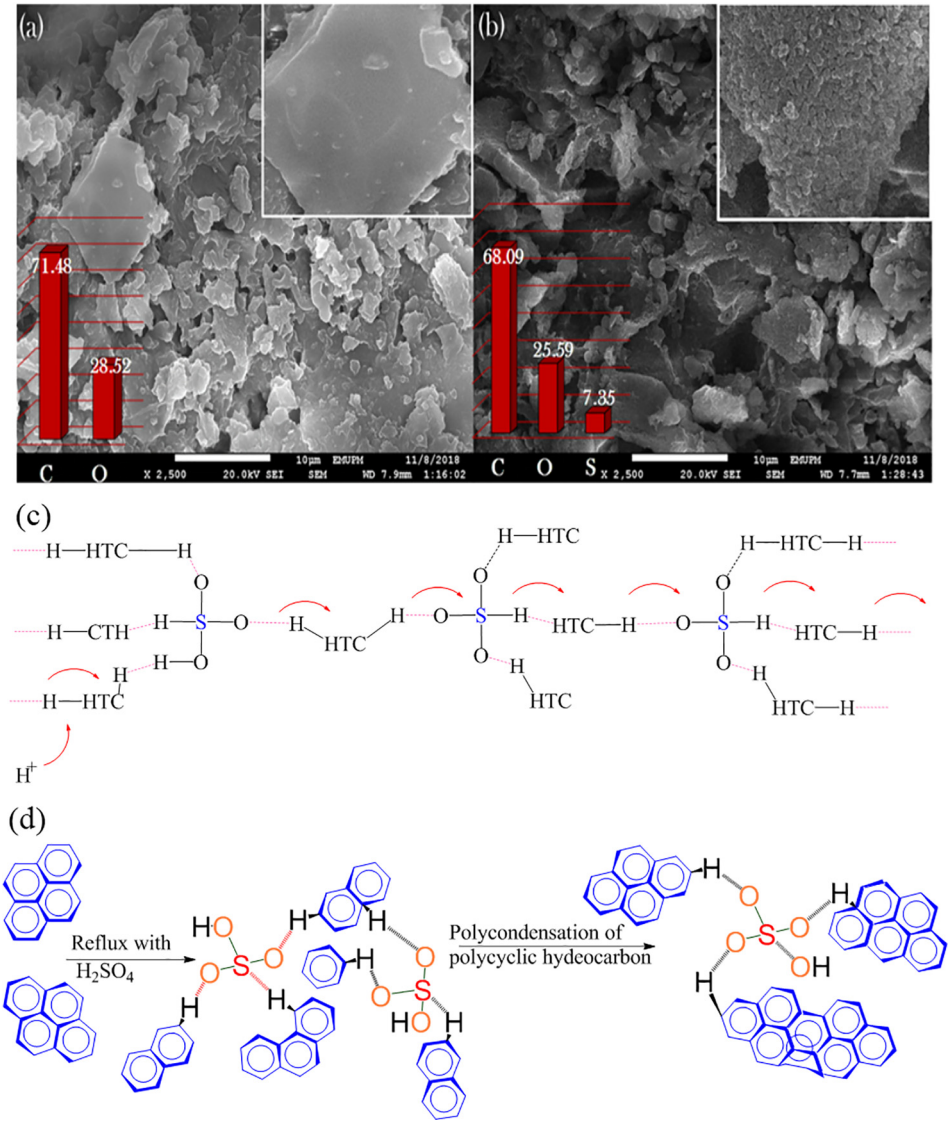

Fig. 3. FESEM and EDX image of (a) HTC catalyst (b) HTC-S catalyst and (c) hydrogen bond network and (d) Grotthuss mechanism.

remarkable increase in acidity of HTC-S was attributed to the attachment of $-SO_3H$ groups to the catalyst surface [30]. According to the FTIR and TPD-NH_3 findings, the distribution of −OH, −COOH, and $-SO_3H$ groups on the HTC surface results in remarkable changes in the acid strength of the catalyst. Because HTC-S features exhibited extensive formation of acidic sites, this catalyst may remarkably promote the esterification of PFAD.

As shown in the Fig. 3a, the FESEM morphology of HTC features showed large aggregates with flat smooth surfaces, which could be due to the destruction and degradation of plants cell walls [31]. An interesting change in surface morphology was observed when HTC was treated with H_2SO_4 (Fig. 3b): the aggregated surface of the catalyst decreased in size and revealed a rougher texture. This change suggests that sulfonation of fragile HTC surfaces can rapidly corrode surface carbon materials [32]. According to the EDX results, the HTC-S catalyst has a sulfur content of 7%, which means $-SO_3H$ groups had successfully linked to the carbon layer as a result of H_2SO_4 treatment and the catalyst is acidic in nature [33]. A Grotthuss mechanism of proton charge transfer has been proposed to explain the structural of HTC-S catalyst. It involved a succession of molecular reorientations via formation of hydrogen bond network at the new transition (Fig. 3c). This mechanism is often assumed in fast proton [34]. The reorganization of hydrogen bonds from excess proton over the hydrogen-bonded network derived H_2SO_4 may result in the structural diffusion and structural defects [35]. Fig. 3d shows the cross-linked structure of carbon layers in HTC obtained after sulfonation treatment. Sulfonation promoted bond cleavage reactions, and HSO_4^- ions form a hydrogen bonding network with carbon through the Grotthuss mechanism. Condensation between polycyclic hydrocarbon fragments after activation with H_2SO_4 may well provide greater dynamic forces for interacting with carbon and contribute to increments in the acidic function of the carbon catalyst [36].

3.2. Esterification of PFAD

The esterification reaction was carried out based on the reported method by lokman et al., [37] with slight modification. The catalytic esterification of PFAD over non-catalyzed (blank) and catalyzed reaction were investigated at 70 °C, 3 wt% catalyst loading, 2 h of reaction, and methanol-to-oil ratio of 15:1; the results are displayed in Fig. 4a. Whereas the blank and HTC exhibited poor esterification efficiency with only 2% and ~6% FFA conversion. HTC-S demonstrated remarkable improvements in esterification activity with ~92% FFA conversion. This result indicates that high esterification activity relies on the high distribution of strong acid sites on a HTC-S catalyst (see TPD-NH_3) [38]. Our findings are in agreement with [39], who attempted the esterification of PFAD over carbon-based solid acid catalysts and

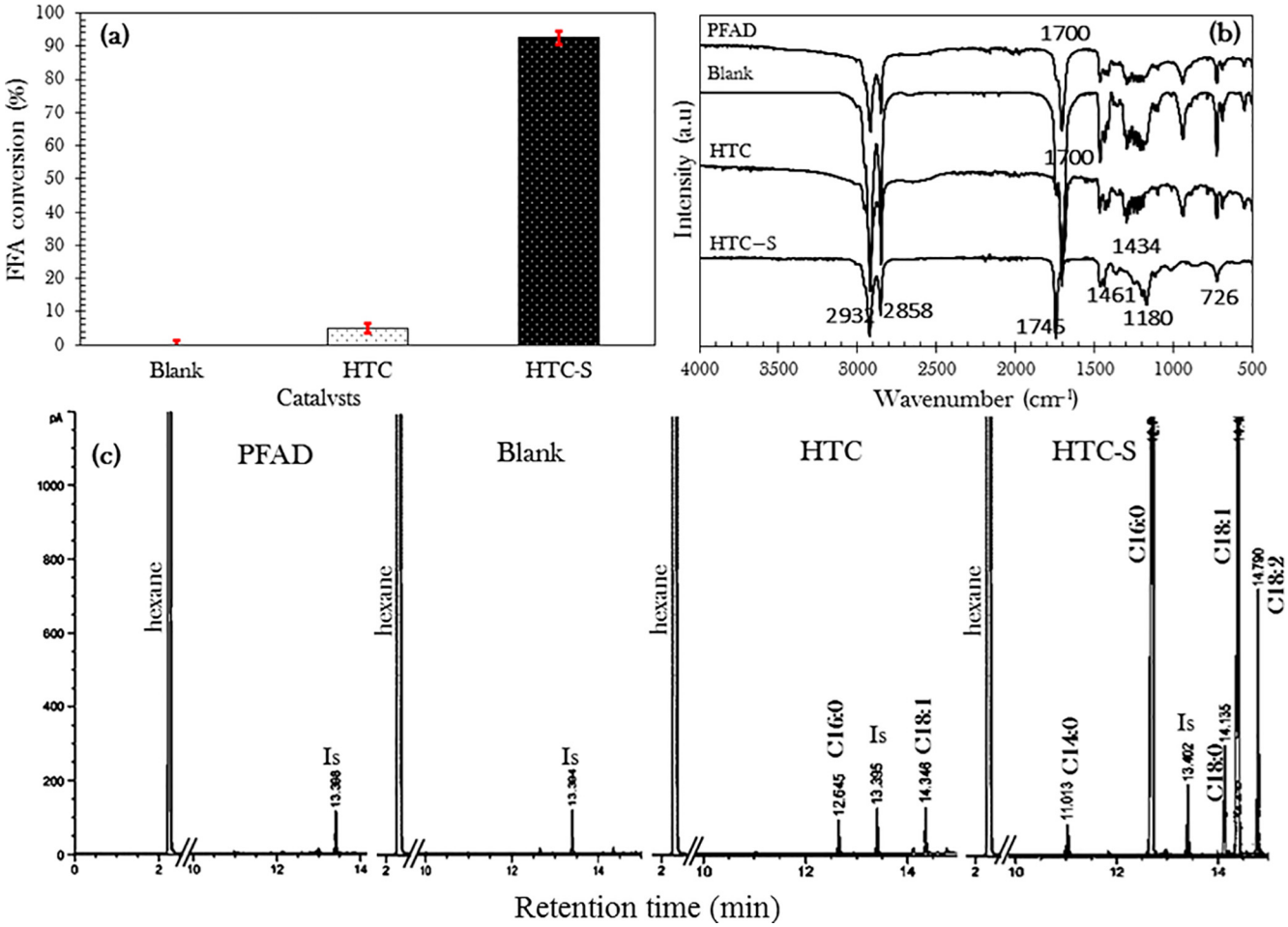

Fig. 4. (a) FFA conversion of catalyzed esterification, (b) FTIR spectra and (c) chromatogram peak for PFAD and biodiesel produced by non-catalyzed and catalyzed esterification reaction at reaction conditions: 70 °C, 3 wt% catalyst loading, 15:1 methanol to PFAD molar ratio and 2 h.

suggested that sulfonation of incompletely carbonized carbohydrates leads to a rigid carbon material consisting of small polycyclic aromatic carbon sheets containing $-SO_3H$ groups. The group further proposed that high esterification activity (90%–93% FFA conversion) is directly related to the higher acidic density of the catalyst. Moreover, $-SO_3H$ could induce the hydrophilicity of the carbon surface, thus allowing methanol molecules to enter the carbon bulk and promoting the esterification reaction in the interior of HTC-S [29]. The surface area and pore properties of the catalysts showed no correlation with their esterification activity's.

The FTIR spectra of the PFAD and biodiesel obtained by non-catalyzed and catalyzed esterification are displayed in Fig. 4b. The absorption peak at 1700 cm^{-1}, which is attributed to −COOH groups in PFAD, dramatically shifted to 1745 cm^{-1}, which is attributed to the ester group (C═O) after catalysis by HTC-S. The presence of $O-CH_3$ stretching in the biodiesel FTIR spectra confirmed by the absorption peak at 1435 cm^{-1} [40]. This finding reveals that complete conversion of carboxylic acid to ester via esterification was achieved by using the HTC-S catalyst [41]. No ester group was detected in the biodiesel produced by blank and HTC-catalyzed esterification, which directly confirms that blank and HTC catalyst can only weakly esterify PFAD. Fig. 4c illustrates chromatograms peak for the PFAD and biodiesel produced from the non-catalyzed and catalyzed esterification reactions. High esterification activity was observed in the HTC-S catalyzed system. The effectiveness of the HTC-S catalyst in promoting the esterification of PFAD was strongly affirmed by the formation of five intense peaks belong to palmitic acid, oleic acid, linoleic acid, stearic acid, and myristic acid methyl esters with a total FAME yield of 85%. Meanwhile, the products obtained by blank and HTC-catalyzed esterification only accounted for 1.2% and 3.8% of the FAME yield. Since the PFAD mainly consists of palmitic acid and oleic acid (Table 1), the FAMEs obtained via HTC-S-catalyzed esterification are predominantly composed of palmitic acid methyl ester (~49%) and oleic acid methyl ester (~22%). The pronounced FAME peak observed after HTC-S catalyzed esterification is comparable with Lokman's finding and implies that the HTC-S catalyst can efficiently drive esterification activity and increase the formation of biodiesel [24].

3.3. Optimization of the esterification reaction using the one-variable-at-a-time approach

The OVAT approach was used to investigate the significance of several factors influencing esterification on PFAD conversion. Several researchers reported that OVAT method can be more effective than fractional factorials technique such as response surface methodology (RSM)-whereas OVAT method only involve limited number of runs and experimental error is not large compared to RSM and the factor is independent from each other [42]. Due to these reasons, OVAT method is used for investigating the effects of four factors, namely, PFAD-to-methanol molar ratio, reaction temperature, reaction time, and catalyst loading, on the esterification of PFAD over the HTC-S catalyst. According to the stoichiometric equation of the esterification reaction, one mole of alcohol and one mole of PFAD are required to produce one mole of FAMEs and water. Higher equilibrium conversion can be obtained if the backward reaction is minimized by using excess methanol as a reactant and shifting the equilibrium to the right-hand side, which

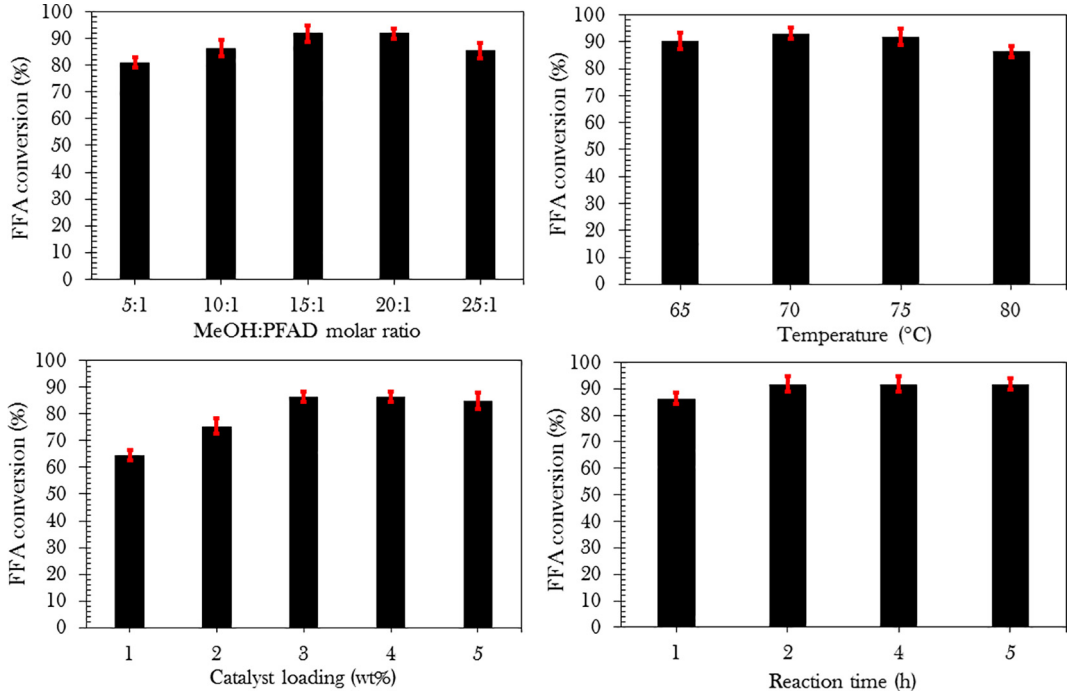

Fig. 5. FFA conversion for esterification of PFAD over HTC-S catalyst prepared using different optimization parameter (a) Effect of methanol to PFAD molar ratio, reaction conditions: 3 wt% catalyst loading, 80 °C, 4 h (b) Effect of reaction temperature, reactions conditions: 3 wt% catalyst loading, 4 h, 15:1 methanol to PFAD molar ratio (c) Effect of HTC-S catalyst loading, reaction conditions: 70 °C, 15:1 methanol to PFAD molar ratio, 4 h (d) Effect of reaction time, reaction conditions: 3 wt%, catalyst loading, 70 °C, 15:1 methanol to PFAD molar ratio.

produces biodiesel. However, excessive addition of methanol could increase the water content of the system and raise the cost of production [43]. Due to these reasons, the effect of PFAD-to-methanol molar ratio on FFA conversion was investigated by varying this molar ratio from 1:5 to 1:25. As seen in Fig. 5a, FFA conversion increased as the PFAD-to-methanol molar ratio increased from 1:5 to 1:15 because a larger amount of methanol provides more opportunities to interact with the molecules of palm fatty acids. However, FFA conversion remarkably decreased when the PFAD-to-methanol molar ratio was further increased to 1:20 and 1:25, possibly because the higher water content in the system and excess alcohol may dilute the reaction mixture and inhibit the esterification reaction [44]. Excess methanol molecules may flood the active sites of the catalyst and hinder the protonation of PFAD [45]. The most suitable PFAD-to-methanol molar ratio is 1:15; using this ratio, a maximum FFA conversion rate of 89% may be obtained.

Mass transfer limitation is regarded as one of the main challenges for esterification reaction and is typically highly correlated with high reaction viscosity [40]. It has been suggested that raising the reaction temperature is the possible solution for overcoming the mass transfer limitation between wax PFAD, methanol and catalyst [46]. Due to this reason, the effect of reaction temperatures ranging from 65 °C to 80 °C on PFAD conversion was studied, and the results are displayed in Fig. 5b. Raising the reaction temperature from 65 °C to 70 °C increased FFA conversion from 88% to 92%; however, a reaction temperature of 80 °C caused a decrease in FFA conversion to 90%. High FFA conversion at the temperature range of 65–70 °C may be attributed to increase in the reaction rate and the improvement of the mass transfer limitation between the reactants and catalyst [43]. On the basis of this finding it can be suggested that as the reaction temperature increases, the viscosity of the distillate decreases, the miscibility between oil and methanol increases, and FFA conversion is enhanced. The reduction in FFA conversion from 70 °C to 80 °C could be the result of the adverse effect of methanol vaporization during the catalytic reaction [47]. Thus, 70 °C appears to be optimum reaction temperature for the present system. The activation energy at 70 °C is adequate to protonate the carbonyl groups of FFAs, resulting in maximum reaction rates [30].

Fig. 5c shows the effect of HTC-S catalyst loading within the range of 1 wt%–5 wt% on FFA conversion. FFA conversion increased from 65% to 88% as the amount of catalyst increased up to 3 wt%. Further increases in catalyst loading resulted in a slight decrement of FFA conversion (87%). The system with 1 wt% catalyst loading showed the lowest FFA conversion due to insufficient catalyst active sites. Increases in catalyst loading improve the availability of active sites in the reaction system and result in increments in number of strong acidic sites. A large number of strongly acidic sites may increase the availability of H^+ during the esterification reaction [48]. However, excess catalyst loading (> 3 wt%) is ineffective to enhance the esterification reaction due to bulk mass fraction [49] and also low contact rate among the catalyst, methanol and feedstock [24]. Excess catalyst may lead to the self-agglomeration of particles, which reduces the availability of actives sites and inhibits FFA conversion [30]. Thus, a catalyst loading of 3 wt % was selected for subsequent experiments on the esterification reaction of PFAD.

The effect of reaction times varying from 1 h to 5 h on FFA conversion was investigated, and the results are shown in Fig. 5d. Reaction for 2 h revealed a steady increase in FFA and provided a maximum conversion rate of 92%. FFA conversion plateaued when the reaction time was increased to 4 h. Similar findings were reported by Hwa et al., who studied the biodiesel production of crude *Jatropha curcas* oil at 65 °C, 15:1 methanol-to-oil molar ratio, and reaction times of 2–6 h; the group obtained FFA conversion rates of 68%–75% at the reaction times studied [50]. This finding suggested that due to the reversibility of the esterification reaction. Overall, 2 h reaction time has been chosen as optimal reaction time for esterification of PFAD.

A mechanism of the esterification of PFAD over HTC-S is proposed in Fig. 6. The acid catalyst mainly provides protons to the esterification reaction. The esterification of PFAD over HTC-S catalyst occurs via several reaction steps: (a) The three oxygen atoms pull the electrons cloud from the sulfur and the hydrogen to make $-SO_3H$ proton donor groups as an active sites, followed by accepting the proton by FFA from

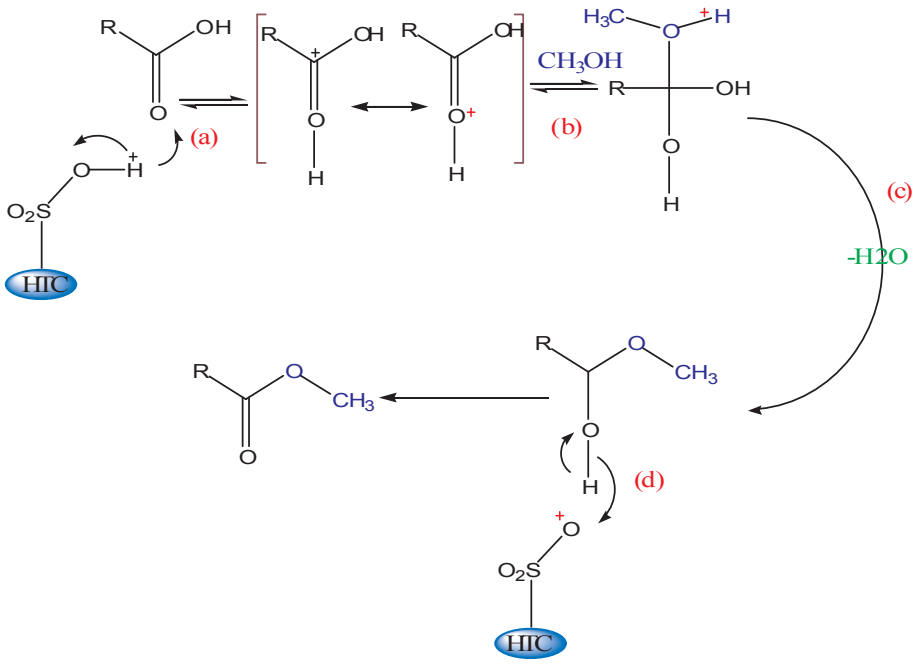

Fig. 6. Proposed mechanism pathways for esterification of PFAD.

the acid catalyst. (b) The alcohol molecule attacks the protonated carbonyl group to yield an intermediate. (c) The intermediate loses a molecule of water to produce a protonated ester. (d) A proton is transferred to the acid catalyst to yield an ester.

3.4. Catalyst reusability and deactivation

The reusability of the HTC-S catalyst was investigated and the spent HTC-S catalyst in each reaction runs were treated via several methods, including: (a) Solvent (hexane and methanol) washing and (b) Hexane washing followed by regeneration with H_2SO_4. As shown in Fig. 7a–b, solvent washing where ineffective techniques to regenerate the catalyst; indeed, esterification activity dramatically decreased and FFA conversion rates of approximately 20% where obtained after the second run of catalyst regenerated in this manner. According to the CHNS analysis of biodiesel obtained, 35% reduction of sulfur species were observed in the second reusability study, thus suggesting that $-SO_3H$ groups are removed from the surface of HTC-S during the reaction. Elimination of $-SO_3H$ from the HTC-S surface could result in the loss of strongly acidic sites and lead to reduction in its esterification activity [51].

Recently, regeneration of carbon catalyst via acid treatment has been reported to maintain the ideal proportion of $-SO_3H$ ions attached to the carbon [46]. According to former study, new $-SO_3H$ sites must be created on used carbon-based catalysts in order to maintain the active sites of the catalyst. Sangar et al., studied the reusability of carbon-derived glycerol (CG) for esterification of PFAD and found that esterification activity is improved and biodiesel production is consistently maintaining at > 96% when the used CG catalyst is subjected to H_2SO_4 (98% purity) regeneration treatment [47]. These findings suggest that maximization the $-SO_3H$ ion proportion on the used HTC-S catalyst is a key factor influencing its esterification activity. The high FFA conversion (90–92%) obtained over two consecutive runs shown in Fig. 7c confirms that regeneration of spent HTC-S catalyst by using H_2SO_4 (98% purity) is highly effective and suitable for biodiesel production. Noteworthy to mention that high FFA conversion is achieved when HTC-S catalyst was regenerated by high concentrated H_2SO_4 (98% purity) than mildly concentrated H_2SO_4 (5% purity). These results confirmed that concentrated H_2SO_4 has a positive role in the existence high numbers of $-SO_3H$ species (negatively charged acidic sites) sites on HTC-S catalyst and simultaneously facilitate the esterification activity. A slight reduction in FFA conversion was observed after the third runs Fig. 8a. This finding could indicate that the remarkable loss of mass catalyst after several consecutive usage has negative impact on the creation of equal proportion active sites like fresh HTC-S catalyst. The reduction mass of used HTC-S catalyst in each reaction runs also implies that the HTC-S catalyst suffered with sulfur leaching (Fig. 8b). Kefas's and Asikin's studies also noted loss of used catalyst mass during production of biodiesel due to the leaching the active species [52,30]. This is further supported with the characterization results from the FESEM-EDX whereas about 30% of reduction of sulfur species have been observed on the third repeated use of spent HTC-S catalyst (Fig. 9). Since, the regenerated H_2SO_4-treated HTC-S can be reused up to two times with FFA conversion > 90%, thus it strongly suggested that HTC-S regenerated by H_2SO_4 (with 98% purity) is still a very promising regeneration catalyst technique as compared to solvent washing.

Researchers have speculated that thermal treatment of the sulfonated carbon catalyst at low temperature is effective in improving its catalyst stability [48]. This finding suggests that low thermal treatment temperature is required to form a rigid carbon framework along with strong attachment $-SO_3H$ acid group on carbon, thus improve the stability of H_2SO_4 treated carbon catalyst. Due to this reason, the fresh HTC-S catalyst was thermally treated at 100, 200, and 300 °C for 2 h under inert conditions. The reusability of the thermally treated HTC-S catalyst was then studied, and the results are shown in Fig. 7d. Interestingly, 100 °C thermal treatment resulted in high esterification activity within range of 70–91% FFA conversion during the first and second runs and but only 25% conversion in the third runs. This finding suggests that 100 °C thermal treatment is beneficial for improving the stability of the HTC-S catalyst. High-thermal treatment temperature (> 200 °C) of HTC-S catalyst for regenerated catalysts showed poor effects. Specifically, HTC-S catalysts treated at 200 °C thermal treatment yielded only 88% of FFA conversion in the first and 24% for second runs, while HTC-S catalysts treated at 300 °C thermal treatment yielded only 7% and 3% FFA conversion in the first and second runs respectively. These finding suggest that $-SO_3H$ species may be degraded by high temperatures, which results in decreases in acid site density and reduced esterification activity [49]. Lowest FFA conversion

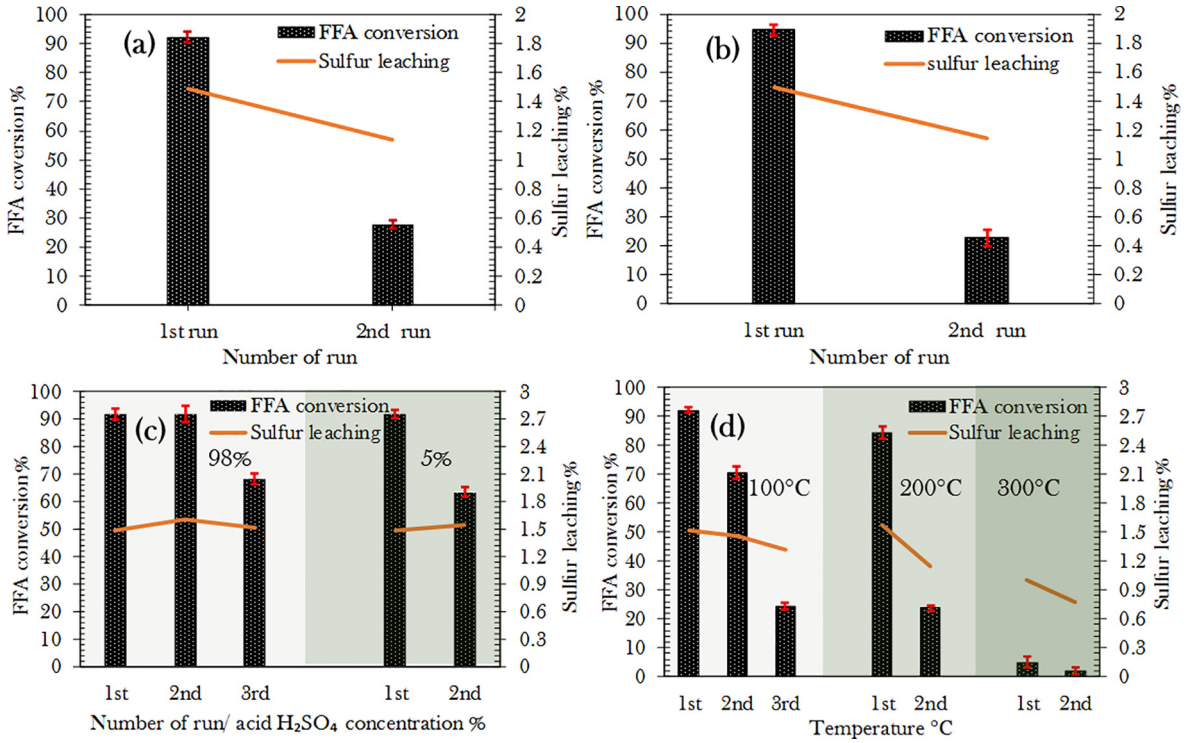

Fig. 7. Reusability test for HTC-S catalyst and amount of sulfur leached with different regeneration method (a) hexane washing (b) methanol washing (c) sulfonation treatment with H_2SO_4 and (d) thermal treatment at 100–300 °C. Reaction condition: 15:1 methanol to PFAD molar ratio, 70 °C reaction temperature, 2 h reaction time and 3 wt% catalyst loading.

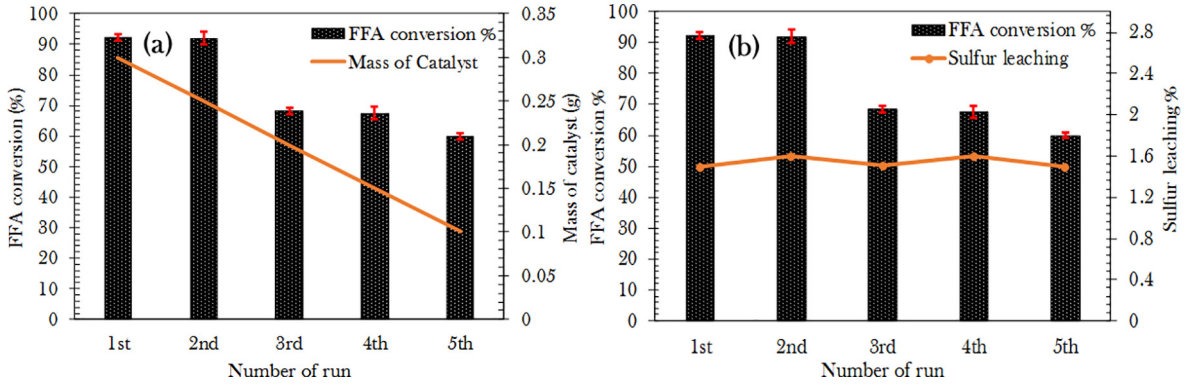

Fig. 8. (a) Reusability vs total mass of the HTC-S catalyst (b) Reusability vs Sulfur leaching of the HTC-S catalyst after H_2SO_4 regeneration treatment (98% purity) at 150 °C for 3 h. Reaction conditions: catalyst amount 3 wt% catalyst loading, 15:1 methanol to PFAD molar ratio, reaction temperature 70 °C, and reaction time 2 h.

and remarkable reduction of the sulfur concentration in the biodiesel obtained from first and second runs of PFAD over HTC-S catalysts treated at 300 °C thermal treatment affirmed this finding.

Based on the solvent washing, H_2SO_4 regeneration treatment and thermal treatment findings revealed that the used HTC-S catalyst stability was appeared to be highly dependent on the regeneration treatment. Both solvent washing and thermal treatment are ineffective for maintaining $-SO_3H$ active sites on the used HTC-S catalyst as compared to H_2SO_4 regeneration technique. Even though, H_2SO_4 regeneration technique can maximize the $-SO_3H$ ion proportion on the used HTC-S catalyst and improved the esterification activity. Yet, this technique is costly as it involves the use of large amount H_2SO_4 (98% purity) whereas not attractive for massive industrial scale. In contrast, catalyst regeneration process via simple solvent washing was considered as the most ideal and quite popular approach in restoring the active sites of used catalyst. This is because the solvent used can be recovered by distillation process—which sustainable for industrial practices. Similarly, thermal treatment technique is simple, yet ineffective since it requires longer preheating times. Overall, any regeneration methods should not be an obstacle in commercializing the HTC-S catalyst, since the raw material for the HTC-S catalyst is derived from waste biomass which is economical than the current industrial homogenous catalyst (KOH, NaOH) [53]. Notably, although regenerated H_2SO_4-treated HTC-S catalyst is capable to be reused up to two consecutive runs with FFA conversion within range of 90–92%, nevertheless, this catalyst is still less efficient than former finding [40,44]. Thus, future work could focus on improving the stability of HTC-S catalysts to enable their industrial applications.

3.5. Fuel properties of PFAD biodiesel and blends PFAD biodiesel

A summary of some physical properties of pure biodiesel (B100) and biodiesel blended petro-diesel produced from the present study are presented in Table 3. The properties were compared to those for biodiesel and diesel outlined in the ASTM D6751 standard. The density at 15 °C of the B10, B30 and B100 are found to be 892 kg/m^3, 864 kg/m^3

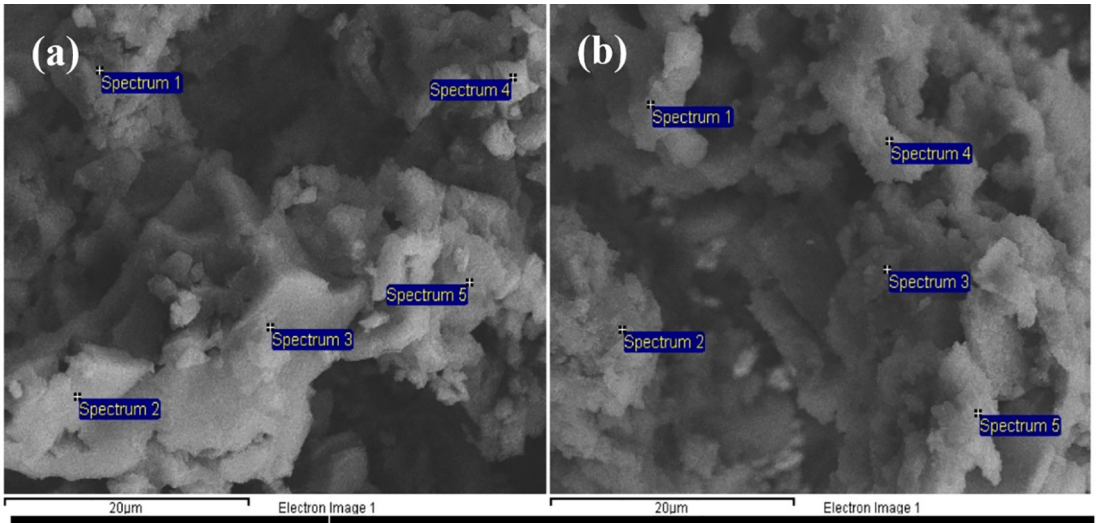

Catalyst	Elemental composition (wt.%)			
	C	O	S	Other*
Fresh HTC-S	69.06±5.41	25.60±6.95	1.13±2.53	4.20±3.51
Spent HTC-S (3rd runs-98% H_2SO_4 treatment)	72.76±5.35	26.01±5.86	0.77±0.19	0.45±0.47

*Other= Mg, Fe and Ca

Fig. 9. FESEM-EDX for (a) fresh and (b) spent HTC-S catalysts.

and 851 kg/m^3, respectively. The density is found to be dependent on the purity of the biodiesel [54], whereby rich biodiesel content resulted in high fuel density. Overall, the density of B10-B100 were close value with ASTM D6751 (870–900 kg/m^3). Notably, the densities of all the biodiesels were found to be higher than diesel. Viscosity is a significant fuel property that could affect the flow and atomization characteristics of a liquid fuel. Typically, high viscosity of fuel may cause poor cold engine start-up and ignition delay [55]. Interestingly, the kinematic viscosity at 40 °C for B10, B30 and B100 are found to be 4.7 mm^2/s, 4.1 mm^2/s and 3.6 mm^2/s, respectively. Compared to the kinematic viscosity of PFAD (96.35 mm^2/s) [56], remarkable reduction of viscosity was observed and this indicated that the effectiveness of catalyzed esterification approach to PFAD feed. Noteworthy to mention, the kinematic viscosity of all biodiesels is found to be higher than diesel, yet, the values were well within the range specified by ASTM D6751 standards. The flash point is the temperature at which the fuel will start to burn when it comes to contact with fire. Thus, high flash point of fuel afforded better safety point of view for easy storage and transportation [57]. The flash point for B100 was determined to be the highest (214 °C) and further reduced with increasing content of petro diesel. The high flash point of B100 is attributed by the presence of predominating unsaturated acid chain length of C18:1 and C18:2 in PFAD Biodiesel [58]. Noted, the flash point for PFAD biodiesel is within ASTM 6751 and majority are higher than diesels, thus it is a safer fuel than diesel. Noteworthy to mention that major disadvantage of biodiesel is its oxygenated compounds may result in thermal instability and rendered poor temperature properties (cloud point and pour point) [59,60]. Interestingly, the low-temperature-properties for B100 and all biodiesel blends still within acceptable ASTM 6751 and diesel standards. Overall, the synthesized PFAD-derived biodiesel in various blends have complied with international biodiesel standard, thus this biodiesel is highly promising for commercialization purposes.

3.6. Summary of studies for carbon-based catalyzed esterification reaction

The summary of the comparison study for the esterification of PFAD over carbon-based catalyst is tabulated in Table 4. It can be seen that HTC-S catalyst exhibited high FFA% (> 90%) and equivalent to former studies [19,20,43,61]. Interestingly, carbon-based catalysts derived from palm kernel shell (PKS) and empty fruit bunch (EFB) exhibited higher esterification activities than the HTC-S catalyst. Nevertheless, the esterification of PFAD using HTC-S is still advantageous as the PFAD successfully converted to biodiesel within shorter reaction (2 h), lower reaction temperature (70 °C) and lower catalyst loading (3 wt%). Even

Table 3
Fuel properties of pure biodiesel, biodiesel blended petro diesel, biodiesel specification and diesel specification.

Property	Unit	ASTM Test method	PFAD Biodiesel			Biodiesel specification[a]	Diesel[b]
			B100	B30	B10		
Density at 15 °C	kg/m^3	D4052	892	864	851	870–900	846
Kinematic viscosity at 40 °C	mm^2/s	D445	4.7	4.1	3.6	1.9–6.0	2.96
Flash point	°C	D93	214	195	143	⩾130	75.5
Pour point	°C	D97	−13	−9	−5	–15 to 10	−35 to − 5
Cloud point	°C	D664	−6	−5	−1		−15 to − 5

[a] Biodiesel specification followed ASTM D6751.
[b] Properties of diesel were obtained from former study [54].

Table 4
Summarized comparison study for esterification of PFAD over carbon-based catalysts.

Catalyst	Type of biomass	Feedstock	Chemical activation	Esterification reaction				FAME conversion (%)	Ref
				T (°C)	t (min)	CL[a] (wt%)	MTPR[b]		
ICS-SO_3H	Starch	PFAD	Conc. H_2SO_4 (98%)	75	180	2%	10:1	94	[19]
PKS-SO_3H	Palm kernel shell (PKS)	PFAD	Chlorosulfonic acid ($ClSO_3H$)	65	60	4	15:1	97	[20]
AC-$Fe_{(x)}$-SO_3Cl	Empty fruit bunch (EFB)	PFAD	Conc. H_2SO_4 (98%)	100	180	4	16:1	98	[61]
SCB	Sugar cane bagasse (SCB)	PFAD	Conc. H_2SO_4 (96%)	170	30	11.5	20:1	80	[43]
HTC-S	Corncob residue	PFAD	Conc. H_2SO_4 (98%)	70	120	3	15:1	92	Present study

[a] CL = catalyst loading.
[b] MTPR = methanol to PFAD molar ratio.

though Chin et al., (2012) successfully produced PFAD biodiesel using SCB catalyst within 30 min, yet the esterification reaction involves high reaction temperature (170 °C), large amount of methanol to oil molar ratio (20:1) and high catalyst loading (11.5 wt%) [43]. Moreover, this study is only achieving 80% FFA conversion, suggesting SCB catalyst is not an ideal option for esterifying the PFAD to biodiesel. Based on the improvised reaction temperature, methanol to oil molar ratio, reaction time and catalyst loading perspective, it can be summarized that HTC-S catalyst is advantageous over ICS-SO_3H, PKS-SO_3H, AC-$Fe_{(x)}$-SO_3Cl and SCB.

4. Conclusions

A heterogeneous solid acid catalyst derived from corncob, HTC-S, was synthesized via hydrothermal carbonization followed by chemical activation using concentrated H_2SO_4. Hydrothermal carbonization maintained the active polar species in the biomass, and H_2SO_4 acid treatment increased the availability of $-SO_3H$ species, thus increasing the strength of acidic sites. HTC-S showed remarkable enhancement of esterification activity with FFA conversion rates of ~92%; these results imply that effective esterification relies on the presence of strong acidic sites in the catalyst. Approximately 92% FFA conversion and 85% FAME yield could be achieved under optimized reaction conditions, which include a 2 h reaction time at 70 °C over 3 wt% catalyst and 15:1 methanol-to-oil molar ratio. The reusability of HTC-S was studied and its stability was appeared to be highly dependent on the regeneration treatment. H_2SO_4 treatment of the spent catalyst offered greater stability and higher FFA conversion rates within the range 90%–92% throughout two consecutive runs. The HTC-S catalyst synthesized via hydrothermal carbonization of corncob and sulfonation treatment has excellent potential use for economical and sustainable biodiesel production.

CRediT authorship contribution statement

S. Fadhilah Ibrahim: Conceptualization, Methodology, Validation, Investigation, Writing - original draft. **N. Asikin-Mijan:** Supervision, Conceptualization, Validation, Writing - original draft, Writing - review & editing. **M. Lokman Ibrahim:** Conceptualization. **G. Abdulkareem-Alsultan:** Investigation, Writing - review & editing. **Saiman Mohd Izham:** Conceptualization. **Y.H. Taufiq-Yap:** Supervision, Funding acquisition.

Declaration of Competing Interest

The authors declare that they have no known competing financial interests or personal relationships that could have appeared to influence the work reported in this paper.

Acknowledgment

The authors acknowledge the financial support from Ministry of Higher Education Malaysia for Fundamental Research Grant Scheme (FRGS 2014-1), Geran Putra Berimpak (GPB) UPM/800-3/3/1/GPB/2018/9658700, Geran Putra Berimpak GBP/2019/9674500.

References

[1] Rocha PD, Oliveira LS, Franca AS. Sulfonated activated carbon from corn cobs as heterogeneous catalysts for biodiesel production using microwave-assisted transesterification. Renew Energy 2019;143:1710–6.
[2] Ayoob AK, Fadhil AB. Valorization of waste tires in the synthesis of an effective carbon based catalyst for biodiesel production from a mixture of non-edible oils. Fuel 2020;264:116754.
[3] Damanik N, Ong HC, Chong WT, Silitonga AS. Biodiesel production from Calophyllum inophyllum – palm mixed oil. Energy Sources, Part A Recover Util Environ Eff 2017;39:1283–9.
[4] Yaakob Z, Mohammad M, Alherbawi M, Alam Z, Sopian K. Overview of the production of biodiesel from Waste cooking oil. Renew Sustain Energy Rev 2013;18:184–93.
[5] Correia LM, de Sousa Campelo N, Novaes DS, Cavalcante CL, Cecilia JA, Rodríguez-Castellón E, et al. Characterization and application of dolomite as catalytic precursor for canola and sunflower oils for biodiesel production. Chem Eng J 2015;269:35–43.
[6] Refaat AA. Biodiesel production using solid metal oxide catalysts. Int J Environ Sci Technol 2011;8:203–21.
[7] Rabiah Nizah MF, Taufiq-Yap YH, Rashid U, Teo SH, Shajaratun Nur ZA, Islam A. Production of biodiesel from non-edible Jatropha curcas oil via transesterification using Bi_2O_3–La_2O_3 catalyst. Energy Convers Manag 2014;88:1257–62.
[8] Zabeti M, Wan Daud WMA, Aroua MK. Activity of solid catalysts for biodiesel production: a review. Fuel Process Technol 2009;90:770–7.
[9] Safa Gamal M, Asikin-Mijan N, Arumugam M, Rashid U, Taufiq-Yap YH. Solvent-free catalytic deoxygenation of palm fatty acid distillate over cobalt and manganese supported on activated carbon originating from waste coconut shell. J Anal Appl Pyrolysis 2019. 104690.
[10] Cheryl-Low YL, Theam KL, Lee HV. Alginate-derived solid acid catalyst for esterification of low-cost palm fatty acid distillate. Energy Convers Manag 2015;106:932–40.
[11] Liu T, Li Z, Li W, Shi C, Wang Y. Preparation and characterization of biomass carbon-based solid acid catalyst for the esterification of oleic acid with methanol. Bioresour Technol 2013;133:618–21.
[12] Titirici M, Antonietti M. Chemistry and materials options of sustainable carbon materials made by hydrothermal carbonization. R Soc Chem 2010:103–16.
[13] Soltani S, Rashid U, Yunus R, Taufiq-Yap YH. Biodiesel production in the presence of sulfonated mesoporous $ZnAl_2O_4$ catalyst via esterification of palm fatty acid distillate (PFAD). Fuel 2016;178:253–62.
[14] Abdulkareem-Alsultan G, Asikin-Mijan N, Lee HV, Taufiq-Yap YH. A new route for the synthesis of La-Ca oxide supported on nano activated carbon via vacuum impregnation method for one pot esterification-transesterification reaction. Chem Eng J 2016;304:61–71.
[15] Chen G, Fang B. Preparation of solid acid catalyst from glucose–starch mixture for biodiesel production. Bioresour Technol 2011;102:2635–40.
[16] Santos EM, Teixeira AP de C, da Silva FG, Cibaka TE, Araújo MH, Oliveira WXC, et al. New heterogeneous catalyst for the esterification of fatty acid produced by surface aromatization/sulfonation of oilseed cake. Fuel 2015;150:408–14.
[17] FAO. Food and agriculture data (FAOSTAT). Food Agric Organ United Nations 2018:1–3.
[18] Arancon RA, Barros HR, Balu AM, Vargas C, Luque R. Valorisation of corncob residues to functionalised porous carbonaceous materials for the simultaneous esterification/transesterification of waste oils. Green Chem 2011;13:3162–7.
[19] Lokman IM, Rashid U, Taufiq-Yap YH. Meso- and macroporous sulfonated starch solid acid catalyst for esterification of palm fatty acid distillate. Arab J Chem 2016;9:179–89.
[20] Farabi MSA, Ibrahim ML, Rashid U, Taufiq-Yap YH. Esterification of palm fatty acid distillate using sulfonated carbon-based catalyst derived from palm kernel shell and bamboo. Energy Convers Manag 2019;181:562–70.
[21] Kitano M, Arai K, Kodama A, Kousaka T, Nakajima K, Hayashi S, et al. Preparation of a sulfonated porous carbon catalyst with high specific surface area. Agris

2009:242–9.
[22] Chellappan S, Nair V, Sajith V, Aparna K. Synthesis, optimization and characterization of biochar based catalyst from sawdust for simultaneous esterification and transesterification. Chinese J Chem Eng 2018;26:2654–63.
[23] Ahmad J, Rashid U, Patuzzi F, Baratieri M, Taufiq-Yap YH. Synthesis of char-based acidic catalyst for methanolysis of waste cooking oil: An insight into a possible valorization pathway for the solid by-product of gasification. Energy Convers Manag 2018;158:186–92.
[24] Lokman IM, Rashid U, Taufiq-Yap YH, Yunus R. Methyl ester production from palm fatty acid distillate using sulfonated glucose-derived acid catalyst. Renew Energy 2015;81:347–54.
[25] Dora S, Bhaskar T, Singh R, Naik DV, Adhikari DK. Effective catalytic conversion of cellulose into high yields of methyl glucosides over sulfonated carbon based catalyst. Biresour. Technol. 2012;120.
[26] Zhang S, Liu S, Yu D, Wang C, Li Q. Preparation and characterization of activated carbon for separation of CO2. Zhongguo Kuangye Daxue Xuebao/J China Univ Min Technol 2014;43:910–4.
[27] Zhang Y, Wong W-T, Yung K-F. Biodiesel production via esterification of oleic acid catalyzed by chlorosulfonic acid modified zirconia. Appl Energy 2014;116:191–8.
[28] Dawodu FA, Ayodele O, Xin J, Zhang S, Yan D. Effective conversion of non-edible oil with high free fatty acid into biodiesel by sulphonated carbon catalyst. Appl Energy 2014;114:819–26.
[29] Mardhiah HH, Ong HC, Masjuki HH, Lim S, Pang YL. Investigation of carbon-based solid acid catalyst from Jatropha curcas biomass in biodiesel production. Energy Convers Manag 2017;144:10–7.
[30] Kefas HM, Yunus R, Rashid U, Taufiq-Yap YH. Modified sulfonation method for converting carbonized glucose into solid acid catalyst for the esterification of palm fatty acid distillate. Fuel 2018;229:68–78.
[31] Xiao L-P, Shi Z-J, Xu F, Sun R-C. Hydrothermal carbonization of lignocellulosic biomass. Bioresour Technol 2012;118:619–23.
[32] Zhou Y, Niu S, Li J. Activity of the carbon-based heterogeneous acid catalyst derived from bamboo in esterification of oleic acid with ethanol. Energy Convers Manag 2016;114:188–96.
[33] Akinfalabi S-I, Rashid U, Yunus R, Taufiq-Yap YH. Synthesis of biodiesel from palm fatty acid distillate using sulfonated palm seed cake catalyst. Renew Energy 2017;111:611–9.
[34] Arribart H, Piffard Y. Indication from NMR of Grotthuss mechanism for proton conduction in $H_2Sb_4O_{11}{\cdot}nH_2O$. Solid State Commun 1983;45:571–5.
[35] Lagodzinskaya GV, Yunda NG, Manelis GB. H+-catalyzed symmetric proton exchange in neat liquids with a network of N-H···N and O–H···O hydrogen bonds and molecular mechanism of Grotthuss proton migration. Chem Phys 2002;282:51–61.
[36] García-Gil J, Ceppi S, Velasco M, Polo A, Senesi N. Long-term effects of amendment with municipal solid waste compost on the elemental and acidic functional group composition and pH-buffer capacity of soil humic acids. Geoderma 2004;121:135–42.
[37] Ibrahim ML, Nik Abdul Khalil NNA, Islam A, Rashid U, Ibrahim SF, Sinar Mashuri SI, et al. Preparation of Na_2O supported CNTs nanocatalyst for efficient biodiesel production from waste-oil. Energy Convers Manag 2020;205:112445.
[38] Tao M-L, Guan H-Y, Wang X-H, Liu Y-C, Louh R-F. Fabrication of sulfonated carbon catalyst from biomass waste and its use for glycerol esterification. Fuel Process Technol 2015;138:355–60.
[39] Huang M, Luo J, Fang Z, Li H. Biodiesel production catalyzed by highly acidic carbonaceous catalysts synthesized via carbonizing lignin in sub- and super-critical ethanol. Appl Catal B Environ 2016;190:103–14.
[40] Fadhil AB, Nayyef AW, Sedeeq SH. Valorization of mixed radish seed oil and Prunus armeniaca L. oil as a promising feedstock for biodiesel production: evaluation and analysis of biodiesels. Asia-Pacific J Chem Eng 2019:1–15.
[41] Nabi MN, Hoque SMN, Akhter MS. Karanja (Pongamia Pinnata) biodiesel production in Bangladesh, characterization of karanja biodiesel and its effect on diesel emissions. Fuel Process Technol 2009;90:1080–6.
[42] Taylor P, Daniel C, Daniel C. One-at-a-time plans one-at-a-time plans. J Am Statist Assoc 2012:37–41.
[43] Chin LH, Abdullah AZ, Hameed BH. Sugar cane bagasse as solid catalyst for synthesis of methyl esters from palm fatty acid distillate. Chem Eng J 2012;183:104–7.
[44] Yujaroen D, Goto M, Sasaki M, Shotipruk A. Esterification of palm fatty acid distillate (PFAD) in supercritical methanol: Effect of hydrolysis on reaction reactivity. Fuel 2009;88:2011–6.
[45] Syazwani ON, Rashid U, Mastuli MS, Taufiq-Yap YH. Esterification of palm fatty acid distillate (PFAD) to biodiesel using Bi-functional catalyst synthesized from waste angel wing shell (Cyrtopleura costata). Renew Energy 2019;131:187–96.
[46] Farooq M, Ramli A, Naeem A. Biodiesel production from low FFA waste cooking oil using heterogeneous catalyst derived from chicken bones. Renew Energy 2015;76:362–8.
[47] Theam KL, Islam A, Lee HV, Taufiq-Yap YH. Sucrose-derived catalytic biodiesel synthesis from low cost palm fatty acid distillate. Process Saf Environ Prot 2015;95:126–35.
[48] Gupta AR, Rathod VK. Solar radiation as a renewable energy source for the biodiesel production by esterification of palm fatty acid distillate. Energy 2019;182:795–801.
[49] Thushari I, Babel S. Sustainable utilization of waste palm oil and sulfonated carbon catalyst derived from coconut meal residue for biodiesel production. Bioresour Technol 2018;248.
[50] Hwa S, Rashid U, Taufiq-yap YH. Biodiesel production from crude Jatropha Curcas oil using calcium based mixed oxide catalysts. Fuel 2014;136:244–52.
[51] Ngaosuwan K, Goodwin JG, Prasertdham P. A green sulfonated carbon-based catalyst derived from coffee residue for esterification. Renew Energy 2016;86:262–9.
[52] Asikin-Mijan N, Lee HV, Taufiq-Yap YH. Synthesis and catalytic activity of hydration–dehydration treated clamshell derived CaO for biodiesel production. Chem Eng Res Des 2015;102:368–77.
[53] Singh D, Sharma D, Soni SL, Sharma S, Sharma PK. Review article A review on feedstocks, production processes, and yield for different generations of biodiesel. Fuel 2020;262:116553.
[54] Dharma S, Masjuki HH, Ong HC, Sebayang AH, Silitonga AS, Kusumo F, et al. Optimization of biodiesel production process for mixed Jatropha curcas–Ceiba pentandra biodiesel using response surface methodology. Energy Convers Manag 2016;115:178–90.
[55] Abbaszaadeh A, Ghobadian B, Omidkhah MR, Najafi G. Current biodiesel production technologies: a comparative review. Energy Convers Manag 2012;63:138–48.
[56] Firdaus M, Yusoff M, Bahadi M. Physical characteristics of palm fatty acid distillate. J Chem Pharm Sci 2019;12:1–5.
[57] Demirbas A. Progress and recent trends in biodiesel fuels. Energy Convers Manag 2009;50:14–34.
[58] Ong HC, Silitonga AS, Masjuki HH, Mahlia TMI, Chong WT, Boosroh MH. Production and comparative fuel properties of biodiesel from non-edible oils: Jatropha curcas, Sterculia foetida and Ceiba pentandra. Energy Convers Manag 2013;73:245–55.
[59] Asikin-Mijan N, Lee HV, Marliza TS, Taufiq-Yap YH. Pyrolytic-deoxygenation of triglycerides model compound and non-edible oil to hydrocarbons over SiO_2-Al_2O_3 supported NiO-CaO catalysts. J Anal Appl Pyrolysis 2018;129:221–30.
[60] Abdulkareem-Alsultan G, Asikin-Mijan N, Lee HV, Rashid U, Islam A, Taufiq-Yap YH. Review on thermal conversion of plant oil (Edible and inedible) into green fuel using carbon-based nanocatalyst. Catalysts 2019;9:1–25.
[61] Ibrahim NA, Rashid U, Taufiq-Yap YH, Yaw TCS, Ismail I. Synthesis of carbonaceous solid acid magnetic catalyst from empty fruit bunch for esterification of palm fatty acid distillate (PFAD). Energy Convers Manag 2019;195:480–91.